Mašín, D. (2014). *Géotechnique* **64**, No. 3, 232–238 [http://dx.doi.org/10.1680/geot.13.P.065]

TECHNICAL NOTE

Clay hypoplasticity model including stiffness anisotropy

D. MAŠÍN*

A hypoplastic model for clays is developed to predict anisotropy of very small strain stiffness. The existing hypoplastic model, with explicit formulation of the asymptotic state boundary surface, is combined with an anisotropic form of the stiffness tensor. The resulting model correctly predicts very small strain stiffness anisotropy. Trends in the anisotropy influence on undrained stress paths are also shown to be properly predicted. The model is evaluated using hollow cylinder apparatus experimental data on London Clay taken over from the literature.

KEYWORDS: anisotropy; clays; constitutive relations; stiffness; stress path

INTRODUCTION

Anisotropy of sedimentary clays is such a significant feature of their mechanical behaviour that it cannot be ignored in boundary value problem simulations. For example, Gunn (1993), Addenbrooke *et al.* (1997), Ng *et al.* (2004) and Franzius *et al.* (2005) demonstrated that incorporation of stiffness anisotropy improved predictions of tunnelling problems. In this technical note, the author develops a hypoplastic model for clays incorporating very small strain stiffness anisotropy. Similarly to the underlying hypoplastic models, the model is capable of predicting small strain stiffness non-linearity, recent stress history effects (Atkinson *et al.*, 1990) and large strain asymptotic behaviour (Gudehus & Mašín, 2009; Mašín, 2012a). The model is based on the earlier research by the author, which will only briefly be summarised here owing to limited space. For details of hypoplastic modelling, readers are referred to the cited publications.

Hypoplasticity is an approach to non-linear constitutive modelling of geomaterials. In its general form (Gudehus, 1996), it may be written as

$$\mathring{\boldsymbol{\sigma}} = f_s(\boldsymbol{\mathcal{L}} : \dot{\boldsymbol{\epsilon}} + f_d \mathbf{N}\|\dot{\boldsymbol{\epsilon}}\|) \tag{1}$$

where $\mathring{\boldsymbol{\sigma}}$ and $\dot{\boldsymbol{\epsilon}}$ represent the objective (Zaremba–Jaumann) stress rate and the Euler stretching tensor respectively, $\boldsymbol{\mathcal{L}}$ and $\mathbf{N}$ are fourth- and second-order constitutive tensors, and f_s and f_d are two scalar factors. In hypoplasticity, stiffness predicted by the model is controlled by the tensor $\boldsymbol{\mathcal{L}}$, whereas strength (and asymptotic response in general, see Mašín (2012a)), is governed by a combination of $\boldsymbol{\mathcal{L}}$ and $\mathbf{N}$. Earlier hypoplastic models (such as the models by Von Wolffersdorff (1996) and Mašín (2005)) did not allow the $\boldsymbol{\mathcal{L}}$ formulation to be changed arbitrarily, as any modification of the tensor $\boldsymbol{\mathcal{L}}$ undesirably influenced the predicted asymptotic states. This hypoplasticity limitation was overcome by Mašín (2012c). He developed an approach enabling the asymptotic state boundary surface to be specified independently of the tensor $\boldsymbol{\mathcal{L}}$, and demonstrated this by proposing a simple hypoplastic equivalent of the Modified Cam Clay model. Based on this approach, Mašín (2012b) developed an advanced hypoplastic model for clays. This model will serve as a base model for the current developments.

Manuscript received 26 April 2013; revised manuscript accepted 28 November 2013. Published online ahead of print 29 January 2014. Discussion on this paper closes on 1 August 2014, for further details see p. ii.

* Faculty of Science, Charles University in Prague, Prague, Czech Republic.

MODEL FORMULATION

The model presented in this technical note combines a hypoplastic model from Mašín (2012b) with an anisotropic form of the tensor $\boldsymbol{\mathcal{L}}$ proposed by Mašín & Rott (2013). A similar problem has already been discussed by Kopito & Klar (2013), who incorporated a transversely isotropic stiffness tensor $\boldsymbol{\mathcal{L}}$ into the model by Mašín (2012c). Mašín & Rott (2013) adopted a general, transversely elastic model formulation, which reads (Spencer, 1982; Lubarda & Chen, 2008)

$$\begin{aligned}\boldsymbol{\mathcal{L}} = {} & \frac{1}{2}a_1\mathbf{1}\circ\mathbf{1} + a_2\mathbf{1}\otimes\mathbf{1} + a_3(\mathbf{p}\otimes\mathbf{1} + \mathbf{1}\otimes\mathbf{p}) \\ & + a_4\mathbf{p}\circ\mathbf{1} + a_5\mathbf{p}\otimes\mathbf{p}\end{aligned} \tag{2}$$

where the tensor products represented by '$\otimes$' and '$\circ$' are defined as

$$\begin{aligned}(\mathbf{p}\otimes\mathbf{1})_{ijkl} &= p_{ij}1_{kl} \\ (\mathbf{p}\circ\mathbf{1})_{ijkl} &= \frac{1}{2}(p_{ik}1_{jl} + p_{il}1_{jk} + p_{jl}1_{ik} + p_{jk}1_{il})\end{aligned} \tag{3}$$

where $p_{ij} = n_i n_j$; n_i is a unit vector normal to the plane of symmetry (in sedimentary soils this vector typically represents the vertical direction). a_1 to a_5 in equation (2) represent five material constants. They can be calculated as

$$a_1 = \alpha_E\left(1 - \nu_{pp} - 2\frac{\alpha_E}{\alpha_\nu^2}\nu_{pp}^2\right) \tag{4}$$

$$a_2 = \alpha_E\nu_{pp}\left(1 + \frac{\alpha_E}{\alpha_\nu^2}\nu_{pp}\right) \tag{5}$$

$$a_3 = \alpha_E\nu_{pp}\left(\frac{1}{\alpha_\nu} + \frac{\nu_{pp}}{\alpha_\nu} - 1 - \frac{\alpha_E}{\alpha_\nu^2}\nu_{pp}\right) \tag{6}$$

$$a_4 = \alpha_E\left(1 - \nu_{pp} - 2\frac{\alpha_E}{\alpha_\nu^2}\nu_{pp}^2\right)\frac{1-\alpha_G}{\alpha_G} \tag{7}$$

$$a_5 = \alpha_E\left(1-\frac{\alpha_E}{\alpha_\nu^2}\nu_{pp}^2\right)+1 - \nu_{pp}^2 - 2\frac{\alpha_E}{\alpha_\nu}\nu_{pp}(1+\nu_{pp}) - \frac{2\alpha_E}{\alpha_G}\left(1-\nu_{pp}-2\frac{\alpha_E}{\alpha_\nu^2}\nu_{pp}^2\right) \tag{8}$$

where the anisotropy coefficients α_G, α_E and α_ν are defined as

$$\alpha_G = \frac{G_{pp}}{G_{tp}} \tag{9}$$

$$\alpha_E = \frac{E_p}{E_t} \tag{10}$$

$$\alpha_\nu = \frac{\nu_{pp}}{\nu_{tp}} \tag{11}$$

G_{ij} are shear moduli, E_i are Young's moduli and ν_{ij} are Poisson ratios. Subscript '$_p$' denotes direction within the plane of isotropy (typically the horizontal direction) and subscript '$_t$' denotes the direction transverse to the plane of isotropy (typically the vertical direction).

When compared to the reference model, incorporation of an anisotropic form of $\boldsymbol{\mathcal{L}}$ requires re-evaluation of the factor f_s from equation (1). According to Mašín (2012c), this factor may be quantified by comparing the isotropic unloading formulation of the hypoplastic model with the isotropic unloading line of the pre-defined form

$$\frac{\dot{e}}{1+e} = -\kappa^*\frac{\dot{p}}{p} \tag{12}$$

where e is the void ratio and p represents mean effective stress.

The isotropic version of the model is obtained by algebraic manipulations with equation (1) (for formulation of all model components see Appendix 1)

$$\dot{p} = \left(\frac{p}{\lambda^*} - 2f_s\frac{A_m}{9}\right)\frac{\dot{e}}{1+e} \tag{13}$$

where

$$A_m = \nu_{pp}^2\left(\frac{4\alpha_E}{\alpha_\nu} - 2\alpha_E^2 + 2\frac{\alpha_E^2}{\alpha_\nu^2} - 1\right) + \nu_{pp}\left(\frac{4\alpha_E}{\alpha_\nu} + 2\alpha_E\right) + 2\alpha_E + 1 \tag{14}$$

Comparison of equation (13) with equation (12) then yields

$$f_s = -\frac{3\mathrm{tr}\boldsymbol{\sigma}}{2A_m}\left(\frac{1}{\lambda^*}+\frac{1}{\kappa^*}\right) \tag{15}$$

The proposed model reduces to the reference one for $\alpha_G = \alpha_E = \alpha_\nu = 1$ (note that additional modification of an exponent appearing in the formulation of f_d is proposed, which is detailed in Appendix 1).

To predict very small strain stiffness and recent stress history effects, the model must be combined with the intergranular strain concept by Niemunis & Herle (1997) (see Appendix 2 for its formulation). The very small strain stiffness matrix $\boldsymbol{\mathcal{M}}_0$ then reads

$$\boldsymbol{\mathcal{M}}_0 = m_R f_s \boldsymbol{\mathcal{L}} \tag{16}$$

The shear G_{tp0} component of the tensor $\boldsymbol{\mathcal{M}}_0$ is given by (from equations (2), (14) and (15))

$$G_{tp0} = m_R\frac{9p}{2A_m}\left(\frac{1}{\lambda^*}+\frac{1}{\kappa^*}\right)\frac{\alpha_E}{2\alpha_G}\left(1-\nu_{pp}-2\frac{\alpha_E}{\alpha_\nu^2}\nu_{pp}^2\right) \tag{17}$$

In the present work, the following dependency of G_{tp0} on mean stress p (Wroth & Houlsby, 1985) is considered

$$G_{tp0} = p_r A_g\left(\frac{p}{p_r}\right)^{n_g} \tag{18}$$

where A_g and n_g are parameters and p_r is a reference pressure of 1 kPa. Comparison of equations (17) and (18) yields the following expression for the variable m_R (note that in the original intergranular strain concept formulation, m_R is considered as a parameter; contrarily, in the formulation proposed here, m_R is a variable calculated on the basis of G_{tp0} in equation (18)).

$$m_R = p_r A_g\left(\frac{p}{p_r}\right)^{n_g}\frac{4A_m\alpha_G}{2p\alpha_E}\left(\frac{\lambda^*\kappa^*}{\lambda^*+\kappa^*}\right)\frac{1}{\left(1-\nu_{pp}-2\frac{\alpha_E}{\alpha_\nu^2}\nu_{pp}^2\right)} \tag{19}$$

The complete model formulation is given in Appendices 1 and 2; its finite-element implementation is freely available online, see Gudehus *et al.* (2008).

MODEL CALIBRATION

In this section, the focus is on calibration of material constants that are new with respect to the original model. For calibration of the parameters ϕ_c, N, λ^* and κ^*, readers are referred to Mašín (2012b). As discussed by Mašín & Rott (2013), complete calibration of transversely isotropic elastic models requires five measurements of wave propagation velocities

(*a*) $V_{SH}(0°)$: S-wave velocity propagating in the direction normal to the plane of isotropy
(*b*) $V_{SH}(90°)$: S-wave velocity propagating within the plane of isotropy with in-plane polarisation
(*c*) $V_P(0°)$: P-wave velocity propagating in the direction normal to the plane of isotropy
(*d*) $V_P(90°)$: P-wave velocity propagating within the plane of isotropy
(*e*) $V_P(45°)$: P-wave velocity propagating under inclination of 45° with respect to the plane of isotropy.

The material constants may then be calculated using

$$G_{tp0} = E \tag{20}$$

$$\alpha_G = \frac{C-D}{2E} \tag{21}$$

$$\nu_{pp} = \frac{AD-B^2}{AC-B^2} \tag{22}$$

$$\alpha_\nu = \frac{C+D}{B}\nu_{pp} \tag{23}$$

$$\alpha_E = \frac{B\alpha_\nu^2 - C\alpha_\nu\nu_{pp}(1+\nu_{pp})}{B\nu_{pp}^2} \tag{24}$$

where (from Mavko *et al.*, 2009)

$$C = \rho_t V_P^2(90°) \tag{25}$$

$$D = C - 2\rho_t V_{SH}^2(90°) \tag{26}$$

$$A = \rho_t V_P^2(0°) \tag{27}$$

$$E = \rho_t V_{SH}^2(0°) \tag{28}$$

$$B = -E + \sqrt{4\rho_t^2 V_P^4(45°) - 2\rho_t V_P^2(45°)(C + A + 2E) + (C + E)(A + E)} \tag{29}$$

where ρ_t represents soil density.

The above-mentioned experiments are not routinely performed in geotechnical engineering laboratories. A simpler calibration procedure assumes that at least bender element shear velocity measurements on vertically and horizontally oriented samples are available for calibration of α_G. α_E and α_ν may then be evaluated using empirical correlations proposed by Mašín & Rott (2013). The exponents x_{GE} and $x_{G\nu}$ are defined as

$$\alpha_E = \alpha_G^{(1/x_{GE})} \tag{30}$$

$$\alpha_\nu = \alpha_G^{(1/x_{G\nu})} \tag{31}$$

Based on evaluation of an extensive experimental database, Mašín & Rott (2013) suggested $x_{GE} = 0{\cdot}8$ and $x_{G\nu} = 1$ (note that the classical Graham & Houlsby (1983) model assumes $x_{GE} = 0{\cdot}5$ and $x_{G\nu} = 1$). The remaining parameter ν_{pp} may in this simplified calibration procedure be estimated by trial and error, using large-strain shear stiffness measurements.

EVALUATION OF THE MODEL

The proposed model has been evaluated using extensive experimental data set on London Clay from Imperial College projects by Nishimura (2005), Gasparre (2005), Nishimura *et al.* (2007) and Gasparre *et al.* (2007). They tested undisturbed samples of London Clay from the excavation at Heathrow, Terminal 5. For the material description and details of the experimental procedures, readers are referred to the above-cited publications. The parameters α_G, A_g and n_g were calibrated using resonant column apparatus tests on London Clay. Empirical expressions were adopted for α_E (equation (30)) and α_ν (equation (31)). ν_{pp} was estimated using stress–strain curves of shear tests at large strains. The parameters ϕ_c, λ^* and κ^*, calibrated using data by Gasparre (2005), were taken over from Mašín (2009). The parameter N was adjusted so that the soil overconsolidation manifested by the undrained stress paths was predicted properly. The initial value of void ratio, $e = 0{\cdot}69$, was calculated from the specimen water content and specific gravity provided by Nishimura *et al.* (2007). The remaining intergranular strain parameters were calibrated using stiffness degradation curves by Nishimura (2005). The material parameters adopted in all the simulations are in Tables 1 and 2. Predictions by the proposed model have been compared with predictions by the reference model by Mašín (2005).

In the evaluation, hollow cylinder tests were used on London Clay from the depth of 10·5 m by Nishimura (2005) and Nishimura *et al.* (2007). Two sets of experiments have been simulated. In the first set, the soil was isotropically consolidated to the in-situ effective stress of $p = 323$ kPa (series 'IC' by Nishimura *et al.* (2007)). In the second set, the initial conditions represented the estimated anisotropic in-situ stress state of $p = 323$ kPa and $q = -166$ kPa (series 'AC' by Nishimura *et al.* (2007)). In both cases, the soil was sheared after consolidation under undrained conditions with controlled vertical strain. The total stress path was defined by constant total mean stress and constant values of variables $\alpha_{d\sigma}$ and b. These were defined as

$$\alpha_{d\sigma} = \frac{1}{2}\operatorname{atan}\left(\frac{2\Delta\tau_{z\theta}}{\Delta\sigma_z - \Delta\sigma_\theta}\right) \tag{32}$$

$$b = \frac{\sigma_2 - \sigma_3}{\sigma_1 - \sigma_3} \tag{33}$$

where σ_1, σ_2 and σ_3 are the major, intermediate and minor principal stresses respectively and σ_z, σ_θ and $\tau_{z\theta}$ are rectilinear stress components in the specimen frame of reference (see Nishimura *et al.* (2007)). The value of b represents the contribution of the intermediate principal stress such that, in the standard compression experiment in triaxial apparatus, $b = 0$. Only simulations with $b = 0{\cdot}5$ are presented here for brevity. $\alpha_{d\sigma}$ represents the principal stress inclination revealing soil anisotropy. In the standard triaxial test, $\alpha_{d\sigma} = 0°$ for the vertically trimmed specimen and $\alpha_{d\sigma} = 90°$ for the horizontally trimmed specimen.

Figure 1(a) demonstrates calibration of the parameter α_G and predictions of very small strain stiffness anisotropy. Fig. 1(b) shows secant stiffness $G_{z\theta}$ degradation with shear strain $\gamma_{z\theta}$ in a hollow cylinder test with $\alpha_{d\sigma} = 23°$ and $b = 0{\cdot}5$ and as predicted by the model.

Stress paths of various tests are in the p plotted against $(\sigma_z - \sigma_\theta)/2$ stress space, as shown in Fig. 2. Stress–strain curves (q/p plotted against the principal strain difference $\epsilon_1 - \epsilon_3$) are presented in Fig. 3. The soil anisotropy is revealed by the deviation of the stress path from vertical (constant p). The proposed model predicts the stress path inclination properly for both isotropically and anisotropically consolidated specimens. The stress paths deviate from the experimental results after the peak of q/p, but this may be

Table 1. Parameters of the intergranular strain concept by Niemunis & Herle (1997) adopted in combination with different hypoplastic models

	A_g or m_R	n_g	m_{rat} or m_T	R	β_r	χ
Proposed model	$A_g = 270$	1	$m_{rat} = 0{\cdot}5$	5×10^{-5}	0·08	0·9
Mašín (2005) model	$m_R = 8$	n/a	$m_T = 4$	5×10^{-5}	0·08	0·9

n/a: not applicable.

Table 2. Parameters of the hypoplastic models used in simulations

	ϕ_c	λ^*	κ^*	N	ν_{pp} or r	α_G
Proposed model	21·9°	0·095	0·015	1·19	$\nu_{pp} = 0{\cdot}1$	2
Mašín (2005) model	21·9°	0·095	0·015	1·19	$r = 0{\cdot}3$	n/a

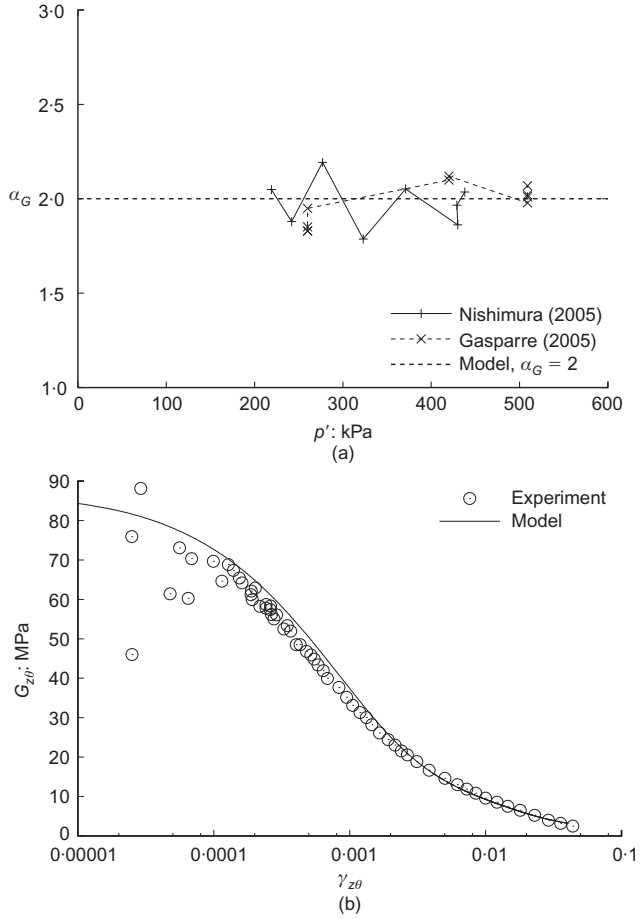

Fig. 1. (a) α_G calibration based on experiments by Nishimura (2005) and Gasparre (2005). (b) Secant shear stiffness degradation as measured by Nishimura (2005) in hollow cylinder test with $\alpha_{d\sigma} = 23^\circ$ and $b = 0{\cdot}5$ and predictions by the proposed model

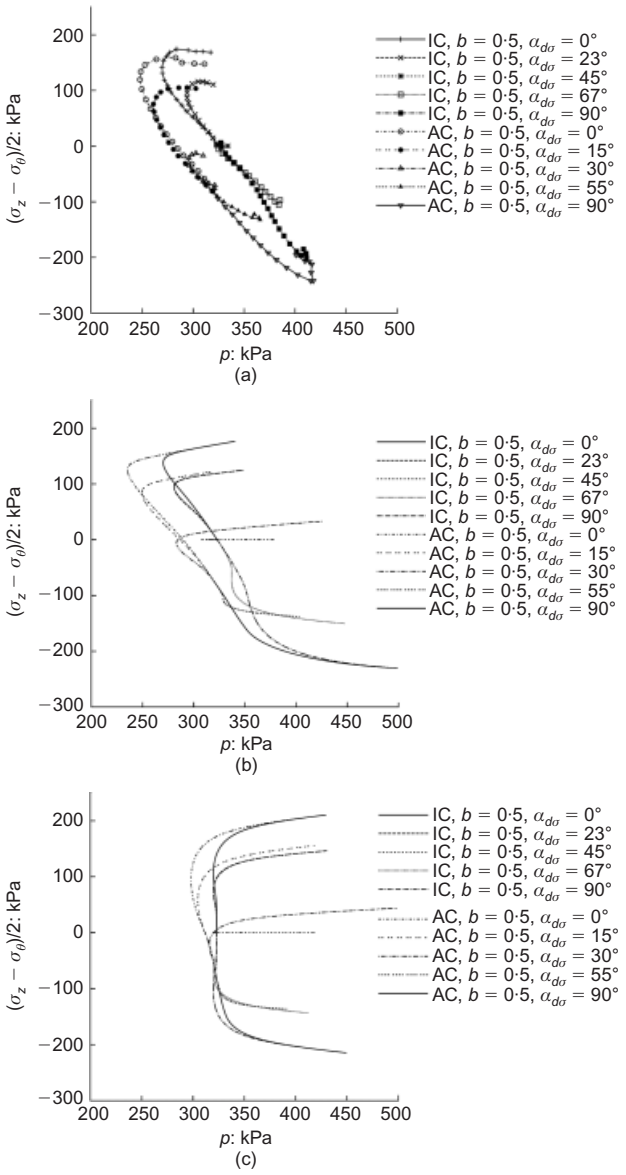

Fig. 2. Stress paths in the p plotted against $(\sigma_z - \sigma_\theta)/2$ stress space: (a) experimental data by Nishimura *et al.* (2007); (b) proposed model; (c) Mašín (2005) model predictions

explained by the specimen rupture and strain localisation into shear bands (see Nishimura *et al.* (2007) for indication of the pre-rupture stress path portions). Predictions by the model by Mašín (2005) are shown in Figs 2(c), 3(e) and 3(f) for comparison. This model predicts some degree of stress-induced anisotropy in the anisotropically consolidated specimens, but its degree cannot be controlled by a parameter and in the present case it is clearly underestimated. The response of the isotropically consolidated specimens is incorrectly predicted as initially isotropic by the Mašín (2005) model.

SUMMARY AND CONCLUSIONS

A new version of the clay hypoplasticity model is developed for predicting stiffness anisotropy. The model is based on the reference model by Mašín (2012b), in which the stiffness tensor $\boldsymbol{\mathcal{L}}$ is replaced by an anisotropic elasticity tensor. The model has been evaluated using a comprehensive data set on London Clay, which includes measurements of the influence of anisotropy in the hollow cylinder apparatus. It is demonstrated that the proposed model predicts not only the influence of anisotropy on the very small strain stiffness, but it also improves predictions of undrained stress paths.

ACKNOWLEDGEMENT

Financial support by the research grant P105/12/1705 of the Czech Science Foundation is greatly appreciated.

APPENDIX 1

Appendix 1 summarises the remaining equations of the proposed hypoplastic model, which have not been specified in the main text.

$$\mathring{\boldsymbol{\sigma}} = f_s \boldsymbol{\mathcal{L}} : \dot{\boldsymbol{\epsilon}} - \frac{f_d}{f_d^A} \boldsymbol{\mathcal{A}} : \mathbf{d} ||\dot{\boldsymbol{\epsilon}}|| \tag{34}$$

$$\boldsymbol{\mathcal{A}} = f_s \boldsymbol{\mathcal{L}} + \frac{\boldsymbol{\sigma}}{\lambda^*} \otimes \mathbf{1} \tag{35}$$

$$f_d = \left(\frac{2p}{p_e}\right)^{\alpha_f} \tag{36}$$

$$p_e = p_r \exp\left[\frac{N - \ln(1+e)}{\lambda^*}\right] \tag{37}$$

$$f_d^A = 2^{\alpha_f}(1 - F_m)^{\alpha_f/\omega} \tag{38}$$

$$F_m = \frac{9I_3 + I_1 I_2}{I_3 + I_1 I_2} \tag{39}$$

$$\omega = -\frac{\ln(\cos^2 \phi_c)}{\ln 2} + a(F_m - \sin^2 \phi_c) \tag{40}$$

$$I_1 = \operatorname{tr} \boldsymbol{\sigma} \tag{41}$$

$$I_2 = \frac{1}{2}[\boldsymbol{\sigma} : \boldsymbol{\sigma} - (I_1)^2] \tag{42}$$

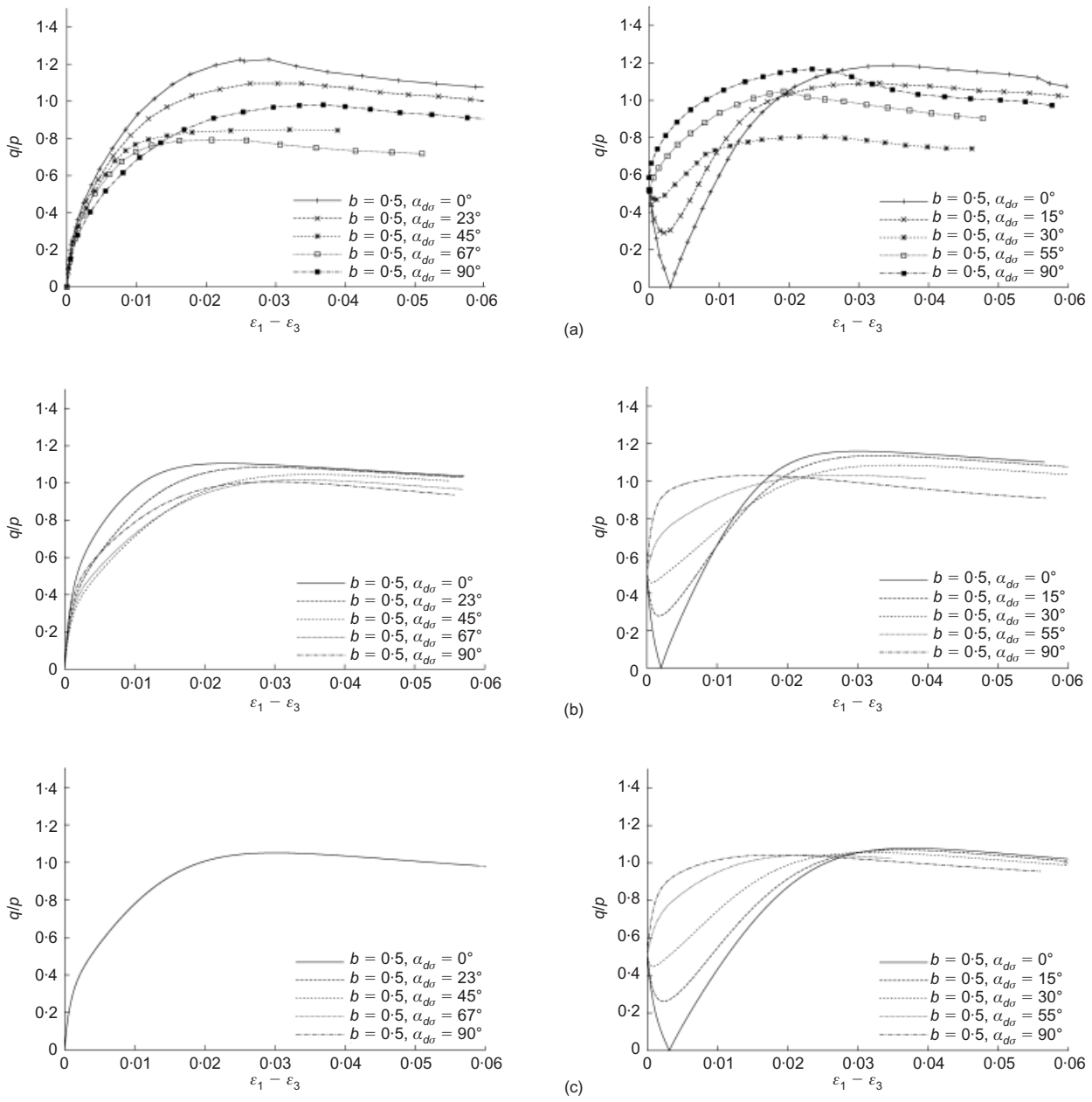

Fig. 3. The ratio q/p plotted against the principal strain difference $\epsilon_1 - \epsilon_3$ for three simulation sets: (a) experimental data by Nishimura *et al.* (2007); (b) proposed model; (c) Mašín (2005) model predictions

$$I_3 = \det \boldsymbol{\sigma} \tag{43}$$

$$\mathbf{d} = \frac{\mathbf{d}^A}{||\mathbf{d}^A||} \tag{44}$$

$$\mathbf{d}^A = -\hat{\boldsymbol{\sigma}}^* + \mathbf{1}\left[\frac{2}{3} - \frac{\cos 3\theta + 1}{4}(F_m)^{1/4}\right] \times \frac{(F_m)^{\xi/2} - \sin^{\xi}\phi_c}{1 - \sin^{\xi}\phi_c} \tag{45}$$

$$\cos 3\theta = -\sqrt{6}\frac{\mathrm{tr}(\hat{\boldsymbol{\sigma}}^* \cdot \hat{\boldsymbol{\sigma}}^* \cdot \hat{\boldsymbol{\sigma}}^*)}{[\hat{\boldsymbol{\sigma}}^* : \hat{\boldsymbol{\sigma}}^*]^{3/2}} \tag{46}$$

$$\xi = 1{\cdot}7 + 3{\cdot}9\sin^2\phi_c \tag{47}$$

$$\hat{\boldsymbol{\sigma}}^* = \frac{\boldsymbol{\sigma}}{\mathrm{tr}\,\boldsymbol{\sigma}} - \frac{\mathbf{1}}{3} \tag{48}$$

The exponent α_f controls irreversibility of the deformation inside the asymptotic state boundary surface. In fact, for high values of α_f the response of the basic model is practically reversible inside the asymptotic state boundary surface, with $f_s\mathcal{L}$ being the stiffness matrix. The model predictions then resemble predictions by the critical state elasto-plastic models. In the reference model by Mašín (2012b), a fixed value of $\alpha_f = 2$ has been suggested. Thorough evaluation of the model's non-linear properties, however, indicated that the α_f value by the Mašín (2005) model leads to better predictions. It is thus suggested to use

$$\alpha_f = \frac{\ln\left[\dfrac{\lambda^* - \kappa^*}{\lambda^* + \kappa^*}\left(\dfrac{3 + a_f^2}{a_f\sqrt{3}}\right)\right]}{\ln 2} \tag{49}$$

$$a_f = \frac{\sqrt{3}(3 - \sin\phi_c)}{2\sqrt{2}\sin\phi_c} \tag{50}$$

In fact, if needed, α_f can be considered as a model parameter controlling the non-linear response inside the asymptotic state boundary surface in the case where ν_{pp} is calibrated rigorously using wave velocity measurements.

The model assumes parameters ϕ_c, λ^*, κ^*, N and ν_{pp}, and state variable e (void ratio). a controls the peak friction angle, and a standard value of $a = 0{\cdot}3$ was suggested by Mašín (2012b). If required, the value of a can be modified to control the peak friction

angle, see Mašín (2012b) for details. α_G, α_E and α_ν are parameters controlling stiffness anisotropy; α_E and α_ν may be approximated using empirical formulations (equations (30) and (31)).

APPENDIX 2

In Appendix 2, the version of the intergranular strain concept used in the proposed model is summarised. The intergranular strain concept was originally proposed by Niemunis & Herle (1997).

$$\mathring{\boldsymbol{\sigma}} = \boldsymbol{\mathcal{M}} : \dot{\epsilon} \tag{51}$$

$$\boldsymbol{\mathcal{M}} = [\rho^{\chi} m_T + (1 - \rho^{\chi}) m_R] f_s \boldsymbol{\mathcal{L}} + \begin{cases} \rho^{\chi}(1 - m_T) f_s \boldsymbol{\mathcal{L}} : \hat{\boldsymbol{\delta}} \otimes \hat{\boldsymbol{\delta}} + \rho^{\chi} f_s f_d \mathbf{N} \hat{\boldsymbol{\delta}} & \text{for } \hat{\boldsymbol{\delta}} : \dot{\epsilon} > 0 \\ \rho^{\chi}(m_R - m_T) f_s \boldsymbol{\mathcal{L}} : \hat{\boldsymbol{\delta}} \otimes \hat{\boldsymbol{\delta}} & \text{for } \hat{\boldsymbol{\delta}} : \dot{\epsilon} \leqslant 0 \end{cases} \tag{52}$$

$$\rho = \frac{\|\boldsymbol{\delta}\|}{R} \tag{53}$$

$$\hat{\boldsymbol{\delta}} = \begin{cases} \boldsymbol{\delta} / \|\boldsymbol{\delta}\| & \text{for } \boldsymbol{\delta} \neq \mathbf{0} \\ \mathbf{0} & \text{for } \boldsymbol{\delta} = \mathbf{0} \end{cases} \tag{54}$$

$$\mathring{\boldsymbol{\delta}} = \begin{cases} (\boldsymbol{\mathcal{I}} - \hat{\boldsymbol{\delta}} \otimes \hat{\boldsymbol{\delta}} \rho^{\beta_r}) : \dot{\boldsymbol{\epsilon}} & \text{for } \hat{\boldsymbol{\delta}} : \dot{\epsilon} > 0 \\ \dot{\boldsymbol{\epsilon}} & \text{for } \hat{\boldsymbol{\delta}} : \dot{\epsilon} \leqslant 0 \end{cases} \tag{55}$$

$$m_R = p_r A_g \left(\frac{p}{p_r}\right)^{n_g} \frac{4 A_m \alpha_G}{2 p \alpha_E} \left(\frac{\lambda^* \kappa^*}{\lambda^* + \kappa^*}\right) \frac{1}{\left(1 - \nu_{pp} - 2 \dfrac{\alpha_E}{\alpha_\nu^2} \nu_{pp}^2\right)} \tag{56}$$

$$m_T = m_{rat} m_R \tag{57}$$

where A_g, n_g, m_{rat}, β_r, χ are parameters and $\boldsymbol{\delta}$ is a state variable.

NOTATION AND CONVENTIONS

Compression negative sign convention is adopted throughout. All stresses are Terzaghi effective stresses unless otherwise stated; the prime symbol is omitted for brevity.

Tensorial operations

$\boldsymbol{\mathcal{L}} : \mathbf{Y}$	inner product $L_{ijkl} Y_{kl}$
$\dot{X}$	rate of X
$\|\mathbf{X}\|$	Euclidean norm $\sqrt{X_{ij} X_{ij}}$
$\mathring{\mathbf{X}}$	objective (Zaremba–Jaumann) rate of $\mathbf{X}$
$\hat{\mathbf{X}}$	tensor normalised by its Euclidean norm $\hat{\mathbf{X}} = \mathbf{X} / \|\mathbf{X}\|$
$\mathrm{tr}\mathbf{X}$	trace operator $1_{ij} X_{ij}$
$\mathbf{X} \otimes \mathbf{Y}$	outer product $X_{ij} Y_{kl}$
$\mathbf{X} \cdot \mathbf{Y}$	inner product $X_{ij} Y_{jk}$
$\mathbf{X} \circ \mathbf{Y}$	tensor product $\frac{1}{2}(X_{ik} Y_{jl} + X_{il} Y_{jk} + X_{jl} Y_{ik} + X_{jk} Y_{il})$

Variables

A, B, C, D, E	parameters of transversely isotropic elasticity model
A_g	parameter quantifying the dependency of G_{tp0} on mean effective stress
A_m	variable in hypoplastic model formulation
a_1, a_2, a_3, a_4, a_5	parameters of transversely isotropic elasticity model
b	variable quantifying the intermediate principal stress magnitude in hollow cylinder apparatus
E_t, E_p	Young moduli ('$_p$' in-plane direction, '$_t$' transversal direction)
e	void ratio
f_d	pyknotropy factor of hypoplastic equation
f_s	barotropy factor of hypoplastic equation
G_{tp}, G_{pp}	shear moduli ('$_p$' in-plane direction, '$_t$' transversal direction)
G_{tp0}	shear modulus at very small strain
$\boldsymbol{\mathcal{L}}$	hypoplasticity fourth-order tensor
$\boldsymbol{\mathcal{M}}_0$	very small strain stiffness tensor
m_R	variable controlling very small strain shear modulus
N	hypoplastic model parameter (position of normal compression line)
$\mathbf{N}$	hypoplasticity second-order tensor
$\mathbf{n}$	unit vector normal to the plane of symmetry
n_g	parameter quantifying the dependency of G_{tp0} on mean effective stress
p	mean effective stress
$\mathbf{p}$	second-order tensor $p_{ij} = n_i n_j$
p_r	reference stress equal to 1 kPa
$V_P(X^\circ)$	P-wave velocity (X° is direction of propagation with respect to axis of symmetry)
$V_{SH}(X^\circ)$	S-wave velocity (X° is direction of propagation with respect to axis of symmetry)
x_{GE}, $x_{G\nu}$	exponents of transversely elastic model formulation
$\alpha_{d\sigma}$	principal stress increment inclination in hollow cylinder test
α_E	anisotropy ratio of Young's moduli
α_G	anisotropy ratio of shear moduli
α_ν	anisotropy ratio of Poisson ratios
ΔX	finite increment of X
ϵ_1, ϵ_3	principal strains (major, minor)
$\dot{\boldsymbol{\epsilon}}$	Euler stretching tensor
κ^*	hypoplastic model parameter controlling volumetric unloading response
λ^*	hypoplastic model parameter (slope of normal compression line)
ν_{tp}, ν_{pp}	Poisson ratios ('$_p$' in-plane direction, '$_t$' transversal direction)
$\boldsymbol{\sigma}$	Cauchy effective stress tensor
σ_1, σ_2, σ_3	principal effective stresses (major, intermediate, minor)
σ_z, σ_θ, $\tau_{z\theta}$	rectilinear effective stress components in the specimen frame of reference in hollow cylinder apparatus
ρ_t	soil density
ϕ_c	critical state friction angle
$\mathbf{1}$	second-order identity tensor

Hypoplasticity specific variables (appearing in appendices only)

$\boldsymbol{\mathcal{A}}$	fourth-order tensor in hypoplastic model formulation
a	hypoplastic variable controlling peak strength, which may be considered as a model parameter
a_f	variable in hypoplastic model formulation
$\mathbf{d}^A$	second-order tensor specifying asymptotic strain rate direction
$\mathbf{d}$	normalised second-order tensor specifying asymptotic strain rate direction
F_m	factor of Matsuoka–Nakai yield condition
f_d^A	pyknotropy factor of hypoplastic equation, asymptotic state value
$\boldsymbol{\mathcal{I}}$	fourth-order identity tensor
I_1, I_2, I_3	effective stress invariants
$\boldsymbol{\mathcal{M}}$	stiffness tensor of the intergranular strain concept formulation
m_T	variable in the intergranular strain concept formulation
p_e	Hvorslev equivalent pressure
R, m_{rat}, β_r, χ	intergranular strain concept parameters
α_f	hypoplastic variable controlling rate of stiffness decrease, may be considered as a model parameter
$\cos 3\theta$	Lode angle function
ξ	variable controlling asymptotic strain rate direction
$\hat{\boldsymbol{\sigma}}^*$	normalised deviator stress
$\boldsymbol{\delta}$	intergranular strain tensor
ρ	normalised intergranular strain tensor magnitude

ω variable controlling asymptotic state boundary surface shape
$\mathbf{0}$ second-order null tensor

REFERENCES

Addenbrooke, T., Potts, D. & Puzrin, A. (1997). The influence of pre-failure soil stiffness on the numerical analysis of tunnel construction. *Géotechnique* **47**, No. 3, 693–712, http://dx.doi.org/10.1680/geot.1997.47.3.693.

Atkinson, J. H., Richardson, D. & Stallebrass, S. E. (1990). Effects of recent stress history on the stiffness of overconsolidated soil. *Géotechnique* **40**, No. 4, 531–540, http://dx.doi.org/10.1680/geot.1990.40.4.531.

Franzius, J. N., Potts, D. M. & Burland, J. B. (2005). The influence of soil anisotropy and K_0 on ground surface movements resulting from tunnel excavation. *Géotechnique* **55**, No. 3, 189–199, http://dx.doi.org/10.1680/geot.2005.55.3.189.

Gasparre, A. (2005). *Advanced laboratory characterisation of London Clay*. PhD thesis, University of London, Imperial College of Science, Technology and Medicine, London, UK.

Gasparre, A., Nishimura, S., Minh, N. A., Coop, M. R. & Jardine, R. J. (2007). The stiffness of natural London Clay. *Géotechnique* **57**, No. 1, 33–47, http://dx.doi.org/10.1680/geot.2007.57.1.33.

Graham, J. & Houlsby, G. T. (1983). Anisotropic elasticity of a natural clay. *Géotechnique* **33**, No. 2, 65–180, http://dx.doi.org/10.1680/geot.1983.33.2.65.

Gudehus, G. (1996). A comprehensive constitutive equation for granular materials. *Soils Found*. **36**, No. 1, 1–12.

Gudehus, G. & Mašín, D. (2009). Graphical representation of constitutive equations. *Géotechnique* **59**, No. 2, 147–151, http://dx.doi.org/10.1680/geot.2007.00155.

Gudehus, G., Amorosi, A., Gens, A., Herle, I., Kolymbas, D., Mašín, D., Muir Wood, D., Nova, R., Niemunis, A., Pastor, M., Tamagnini, C. & Viggiani, G. (2008). The soilmodels.info project. *Int. J. Numer. Analyt. Methods Geomech*. **32**, No. 12, 1571–1572.

Gunn, M. J. (1993). The prediction of surface settlement profiles due to tunnelling. In *Predictive soil mechanics: Proceedings of the Worth Memorial Symposium, London* (eds G. T. Houlsby and A. N. Schofield), pp. 304–316. London, UK: Thomas Telford.

Kopito, D. & Klar, A. (2013). Discussion: Hypoplastic Cam-clay model. *Géotechnique* **63**, No. 10, 889–890, http://dx.doi.org/10.1680/geot.12.D.008.

Lubarda, V. A. & Chen, M. C. (2008). On the elastic moduli and compliences of transversely isotropic and orthotropic materials. *J. Mech. Mater. Structs* **3**, No. 1, 153–171.

Mašín, D. (2005). A hypoplastic constitutive model for clays. *Int. J. Numer. Analyt. Methods Geomech*. **29**, No. 4, 311–336.

Mašín, D. (2009). 3D modelling of a NATM tunnel in high K_0 clay using two different constitutive models. *J. Geotech. Geoenviron. Engng ASCE* **135**, No. 9, 1326–1335.

Mašín, D. (2012a). Asymptotic behaviour of granular materials. *Granular Matter* **14**, No. 6, 759–774.

Mašín, D. (2012b). Clay hypoplasticity with explicitly defined asymptotic states. *Acta Geotechnica* **8**, No. 5, 481–496.

Mašín, D. (2012c). Hypoplastic Cam-clay model. *Géotechnique* **62**, No. 6, 549–553, http://dx.doi.org/10.1680/geot.11.T.019.

Mašín, D. & Rott, J. (2013). Small strain stiffness anisotropy of natural sedimentary clays: review and a model. *Acta Geotechnica*, http://dx.doi.org/10.1007/s11440–013–0271–2.

Mavko, G., Mukerji, T. & Dvorkin, J. (2009). *The rock physics handbook: tools for seismic analysis of porous media*, 2nd edn. New York, USA: Cambridge University Press.

Ng, C. W. W., Leung, E. H. Y. & Lau, C. K. (2004). Inherent anisotropic stiffness of weathered geomaterial and its influence on ground deformations around deep excavations. *Can. Geotech. J.* **41**, No. 1, 12–24.

Niemunis, A. & Herle, I. (1997). Hypoplastic model for cohesionless soils with elastic strain range. *Mech. Cohesive-Frictional Mater.* **2**, No. 4, 279–299.

Nishimura, S. (2005). *Laboratory study on anisotropy of natural London clay*. PhD thesis, University of London, Imperial College of Science, Technology and Medicine, London, UK.

Nishimura, S., Minh, N. A. & Jardine, R. J. (2007). Shear strength anisotropy of natural London Clay. *Géotechnique* **57**, No. 1, 49–62, http://dx.doi.org/10.1680/geot.2007.57.1.49.

Spencer, A. J. M. (1982). The formulation of constitutive equation for anisotropic solids. In *Mechanical behaviour of anisotropic solids* (ed. J. P. Boehler). The Hague, the Netherlands: Martinus Nijhoff Publishers.

Von Wolffersdorff, P. A. (1996). A hypoplastic relation for granular materials with a predefined limit state surface. *Mech. Cohesive-Frictional Mater.* **1**, No. 3, 251–271.

Wroth, C. & Houlsby, G. (1985). Soil mechanics – property characterisation, and analysis procedures. *Proceedings of the 11th international conference on soil mechanics and foundation engineering*, San Francisco, vol. 1, pp. 1–55. Rotterdam, the Netherlands: Balkema.